



NRC Publications Archive Archives des publications du CNRC

Evaluating dense 3D surface reconstruction techniques using a metrological approach

Toschi, Isabella; Beraldin, Jean-Angelo (Angelo); Cournoyer, Luc; De Luca, Livio; Capra, Alessandro

This publication could be one of several versions: author's original, accepted manuscript or the publisher's version. / La version de cette publication peut être l'une des suivantes : la version prépublication de l'auteur, la version acceptée du manuscrit ou la version de l'éditeur.

For the publisher's version, please access the DOI link below. / Pour consulter la version de l'éditeur, utilisez le lien DOI ci-dessous.

Publisher's version / Version de l'éditeur:

<https://doi.org/10.1080/19315775.2015.11721715>

NCSLI Measure : The Journal of Measurement Science, 10, 1, pp. 38-48, 2015-05-01

NRC Publications Record / Notice d'Archives des publications de CNRC:

<https://nrc-publications.canada.ca/eng/view/object/?id=775ea633-bbaa-4f89-8635-6ec7fe104563>

<https://publications-cnrc.canada.ca/fra/voir/objet/?id=775ea633-bbaa-4f89-8635-6ec7fe104563>

Access and use of this website and the material on it are subject to the Terms and Conditions set forth at

<https://nrc-publications.canada.ca/eng/copyright>

READ THESE TERMS AND CONDITIONS CAREFULLY BEFORE USING THIS WEBSITE.

L'accès à ce site Web et l'utilisation de son contenu sont assujettis aux conditions présentées dans le site

<https://publications-cnrc.canada.ca/fra/droits>

LISEZ CES CONDITIONS ATTENTIVEMENT AVANT D'UTILISER CE SITE WEB.

Questions? Contact the NRC Publications Archive team at

PublicationsArchive-ArchivesPublications@nrc-cnrc.gc.ca. If you wish to email the authors directly, please see the first page of the publication for their contact information.

Vous avez des questions? Nous pouvons vous aider. Pour communiquer directement avec un auteur, consultez la première page de la revue dans laquelle son article a été publié afin de trouver ses coordonnées. Si vous n'arrivez pas à les repérer, communiquez avec nous à PublicationsArchive-ArchivesPublications@nrc-cnrc.gc.ca.



Evaluating Dense 3D Surface Reconstruction Techniques using a Metrological Approach

Isabella Toschi¹
toschi@fbk.eu

Jean-Angelo Beraldin²
angelo.beraldin@nrc-cnrc.gc.ca

Luc Courmoyer²
luc.courmoyer@nrc-cnrc.gc.ca

Livio De Luca³
livio.deluca@map.archi.fr

Alessandro Capra⁴
alessandro.capra@unimore.it

¹3D Optical Metrology (3DOM) unit
Bruno Kessler Foundation (FBK)
Via Sommarive 18 I-38123
Povo-Trento, Italy

²National Research Council of Canada (NRC)
1200 Montreal Road
CAN-K1A-0R6
Ottawa, Canada

³CNRS, UMR 3495
Modèles et simulations pour l'Architecture et le Patrimoine (MAP)
31, Chemin Joseph Aiguier, F-13402
Marseille, France

⁴Dept. of Engineering "Enzo Ferrari"
University of Modena and Reggio Emilia
Via Vignolese 905, I-41125
Modena, Italy

Abstract: This paper discusses an approach for evaluating the accuracy of dense 3D surface reconstruction techniques based on images. So far, the emergence of these novel techniques has not been supported by the definition of an internationally recognized standard which is fundamental for user confidence and market growth. In order to provide an element of reflection and solution to the different communities involved in image-based 3D modelling, we present an approach for the assessment of the metric performance of an open-source set of routines for bundle block adjustment and dense image matching (Apero/MicMac). The evaluation is performed using a metrological approach, through comparisons between image-based 3D generated data and ‘reference’ data acquired with two hemispherical laser scanners, one total station, and one laser tracker. Aspects of traceability and measurement uncertainty of all these reference 3D data are discussed. The methodology is applied to two case studies, tailored to analyze the software capabilities in dealing with both outdoor and environmentally controlled conditions. Comparative data and accuracy evidence provided by both tests allow the study of some key factors affecting 3D model accuracy.

1. Introduction

1.1 Context

A number of solutions for the automatic generation of textured dense 3D surface models from 2D images in single/multiple baseline arrangements are now available. In particular, both low cost software packages and open source solutions including web services have become very popular. These solutions provide satisfactory results from a visual point of view, but have the major disadvantage of lacking clear and unambiguous metric results [1]. For instance, in the field of cultural heritage, the strong geometric and visual consistency of a 3D representation is an essential condition for the documentation and analysis of heritage artefacts. This argument can also be said of numerous industrial applications of this technology.

Many publications have looked at accuracy tests results for image-based methods. Most of the comparisons are performed using either ‘reference’ data acquired with active 3D imaging systems (laser or pattern projection) or geometric artefacts with known form and size (spheres, flat plates, and gauge blocks). Although this general approach may be seen as reasonable, the latter approach has a better metrological traceability chain than the former. For instance, roundness measurement on a reference artefact is a well-established technology with a traceability chain. On the other hand, 3D measurements using mobile laser scanners or reconfigurable 3D imaging systems are performed on a regular basis, but internationally recognized standards are nowhere to be found let alone a traceability chain. It is true that manufacturers of those systems provide to their customers a datasheet or a calibration certificate with some numerical values and sometimes a terminology that is close to the *VIM* [2] and the *GUM* [3]. Nevertheless, it is important to understand that these documents are not generated according to an international standard but instead they are linked to internal company guidelines that may or may not be available to the customer. Fortunately, efforts are being made in international organizations like *ASTM (E57)* [4], *ISO/TC 213 (ISO 10360)* [5] and *ISO/TC 172/SC 6 (ISO 17123)* [6] and by the German national body *VDI-VDE (2634)* [7]. Current methods rely on a comparison between a given measurement dataset from one ‘instrument’ and

another measurement dataset from a reference ‘instrument’ that provides measurements with a smaller uncertainty (at least four times smaller as per *ISO 14253* [8]) compared to the instrument being evaluated.

In reality, the user has to be satisfied with an unmediated comparison via dissimilar instrument technologies, or in the absence of a reference ‘instrument’, the use of a reference data set derived from the different data sets under study where some statistical method has been applied to the whole data set in order to find consensus. The metrological approach we use in this paper attempts to fill this void by reviewing the metrological aspects of the problem and by proposing an avenue for solution with dissimilar technologies.

1.2 Review of Approaches for Evaluating Image-based Methods

As shown by the authors in [9], there is a need for accuracy evaluation tools for image-based 3D modelling. Key factors and critical configurations affecting 3D model accuracy are also needed. These authors propose a technique that creates simulated data based on the actual project data. As a result, guidelines for some phases of 3D modelling from images are given. According to the authors, it is difficult to achieve optimum network design in practice. Therefore, the goal should be to strive for strong geometric configurations, high redundancy, high image resolutions on natural features, and correct calibration. The authors in [10] expand the previous work and that of the authors in [11], by proposing a guideline for image data acquisition called “One panorama each step”. The European Spatial Data Research Organisation (EuroSDR) project aims at benchmarking image matching approaches for Digital Surface Models (DSM) computation from airborne imagery [12]. A test bed is proposed to software developers, distributors, and users of dense matching software in order to evaluate on a continuous basis image-based DSM approaches as the technology is improved. Other examples of benchmarks that aim at measuring the performance of different state-of-the-art matching algorithms can be found in [13] and [14].

The authors in [15] compare four independent dense matching packages for scaled surface reconstruction using stereo camera rigs without measuring any object distances. The tests aim at evaluating both the ability to resolve the scale and to assess the reliability in terms of accuracy. It is noted by the authors that laser scanner data are not an absolute reference and therefore the comparisons show relative errors only. A comparison of an automatic photogrammetric technique based on MicMac (*Multi-Images Correspondances, Méthodes Automatiques de Corrélation*) to a terrestrial laser scanning for 3D modelling of a building’s stairway with a height of about 12 m is presented in [16]. The authors conclude that their approach does not reach the geometric quality of a time-of-flight laser scanner, since image-based methods are heavily dependent on the presence of texture (reflectance). Nevertheless, the conclusion is that photogrammetry can be considered an interesting solution thanks to its scalability, low cost, and onsite swiftness.

A critical insight and a metric evaluation of automated image orientation packages are explained in [1]. Different data sets are used in this evaluation. Large and complex scenes with known shapes, precise ground control points (GCPs), calibrated cameras, and reference scale bars are used in the evaluation of the different software packages. The conclusion is that all the

packages evaluated deliver similar results in terms of theoretical precisions of the computed object coordinates and recovered interior camera parameters (in the case of a robust image network). It is interesting to note that in many publications the metric quality of 3D reference coordinates originates from active 3D systems either triangulation [17] or time-of-flight-based [18] and those reference coordinates are seldom questioned.

1.3 MicMac and Associated Tools

For our tests we use the suite of software tools developed by the French mapping agency (IGN – *Institut Géographique National*). This suite includes a number of routines. Among them, Apero and MicMac represent the two main software solutions. The former computes the internal and external orientations of images [19], whereas the latter performs the surface reconstruction by computing depth maps from oriented images [20]. The image-based pipeline consists of three main steps (

Figure 1). The first one (Tapioca tool) is the tie point extraction process which is based on a Sift⁺⁺ implementation of SIFT algorithm [21]. Calibration and orientation are then performed in Apero. As input, the tool can receive inhomogeneous observations, such as tie points, GCPs and camera external orientations measured with on-board sensors (GNSS/IMU). The process makes use of both computer vision techniques, in the initialization phase, and photogrammetric techniques, in the bundle adjustment refinement phase [22]. The two steps are mixed together, in order to avoid undesirable error accumulation and lead the system to convergence. Both pre-calibration input and camera self-calibration are supported with a choice of lens models. Finally, the dense image matching phase is carried out in MicMac. The tool implements a multi-stereo formulation with the NCC (Normalized Cross Correlation) coefficient as the similarity measure. It is specifically adapted to deal with large image datasets. The surface reconstruction is performed with a multi-scale, multi-resolution image matching approach that includes a regularization algorithm based on an energetic formulation.

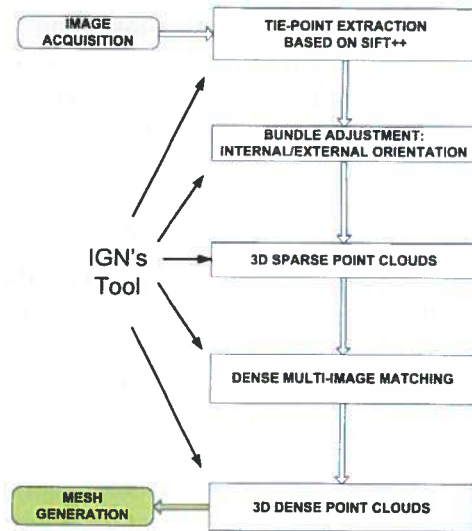


Figure 1. Procedural workflow used to determine a dense point cloud using *Institut Géographique National* of France - IGN's Apero/MicMac software suite.

1.4 Paper Structure

This paper describes an approach designed to evaluate the metric performance of a particular image-based 3D modelling technique with a “metrological approach”. The project is presented in Section 2. The first test is carried out in an outdoor environment, whereas the second one is performed within an environmentally controlled laboratory. For both cases, the performance of the algorithms implemented in the IGN's suite of tools is assessed for single views. In Section 3, a description of the origin of the reference data set is given along with the metrological approach based on an error budget computation. The results summarized in Section 4 are aimed at presenting the metric evaluation of orientation and dense image matching phases. Conclusions are presented in Section 5.

2. Project Description

2.1 Experiment in an Outdoor Environment

The IGN's software suite provides the user with the possibility of finely controlling each process through a large amount of attributes and parameters. This flexibility, however, forces the user to deal with the lack of clear rules and best practices in the software manual. Furthermore, the acquisition protocol doesn't usually follow specific rules, especially in terms of convergence angles and lens focal setting. In order to fill these gaps, different image acquisition protocols are tested and their influence on the orientation and dense matching phases is studied. Moreover, for each step of the procedural workflow (

Figure 2), a set of the most significant software parameters is examined as well, starting from selected acquisition protocols. These parameters include among other things, lens model, regularization parameter, image resolution, and so on [29]. Appropriate reference data described later are employed. The calculation of basic statistical parameters, inspection of error distribution histograms, and computational speed are used in the decision making process to determine the best solution that is then used as input for the subsequent phase.

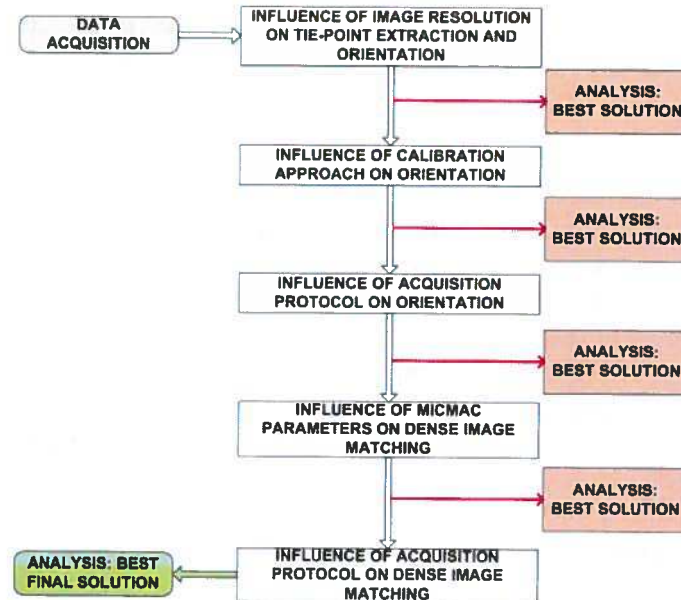


Figure 2. Procedural workflow used to determine the most appropriate software parameters (IGN's suite of tools) in an outdoor environment experiment.

Given the goal of this work, the main entrance of the cathedral of Marseille (Cathédrale de la Major) is chosen as test object (

Figure 3) as it matches the following requirements: significant depth variations, presence of detailed surfaces, different textures, colors and materials (stones, marble and wood), high availability of open space in front of the scene, and outdoor conditions.

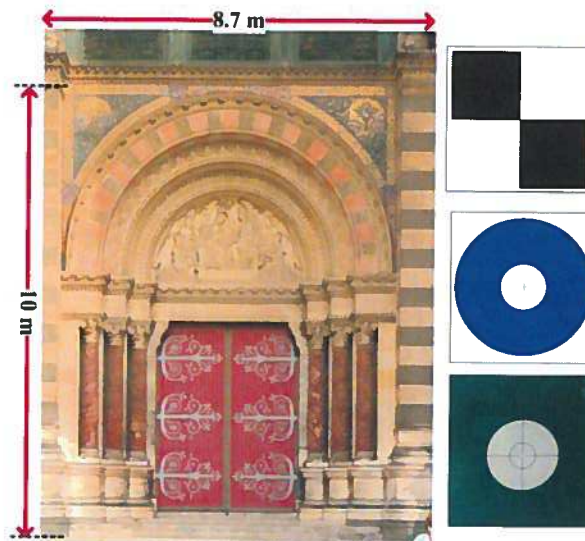


Figure 3. Entrance of the Cathédrale de la Major in Marseille, France, left image: test-object, right image: contrast targets used as control points (coordinates).

The image acquisition phase is performed using a Nikon D3X digital camera (6080×4044 pixels) and two different lenses: a fixed focal length lens (Nikon AF Micro-Nikkor 60 mm f/2.8D) and a zoom-lens, employed at its lowest zoom level (Nikon AF Nikkor 24 to 85 mm f/2.8 4D IF), i.e. 24 mm. Both lenses are not equipped with optical image stabilizers that would impact the lens calibration. For each lens, images are acquired with a cross shape convergent configuration [23], where three different values of convergence angles denoted as α (3° , 5° , 10°) are tested. An image is captured in one position and four supporting images are then captured at approximately equal distance from it; this arrangement replicates a cross shape. The image acquisition does not use rigidly connected cameras on a stable structure. In order to achieve comparable final results, the camera-object distances are selected using design equations and an image interpolation of $1/2$ pixel is assumed so that the resulting range uncertainty and lateral resolution are metrically equivalent [24]. The camera-object distances are 14 m and 26 m for the 24 mm lens and the 60 mm lens, respectively. All acquisition protocols are performed with the same photographic parameter setup, i.e. focusing fixed at infinity, $f/8$ and ISO sensitivity 200.

2.2 Experiment in an Environmentally Controlled Laboratory

An environmentally controlled laboratory offers a privileged context for traceable measurements where the accuracy of a measurement in terms of the uncertainty can be evaluated with limited effects due to temperature, humidity and pressure (*ISO 14253-2*). In a way, such environment provides a setting to determine the best accuracy achievable with a particular software and methodology. Again our attention is focused on the study of different image acquisition protocols and their resulting influence on the algorithm performance as summarized in the procedural workflow of

Figure 4.

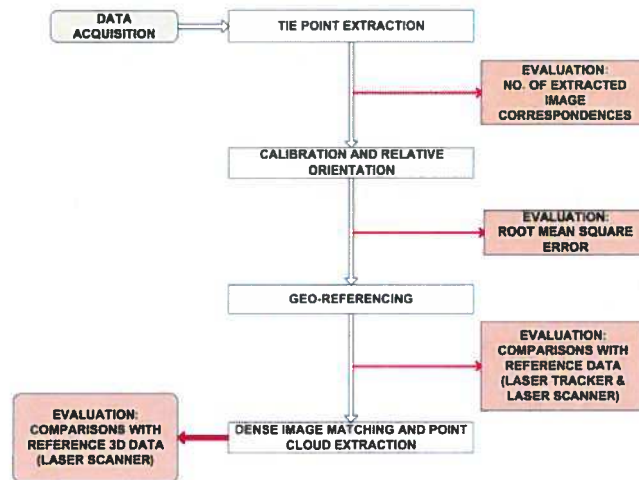


Figure 4. Procedural workflow used to determine the most appropriate software parameters (IGN's suite of tools) for the experiment in an environmentally controlled laboratory at NRC Canada.

Tests are performed within the National Research Council (NRC) of Canada Metrological Laboratory, built specifically for 3D imaging metrology work. Controlled air temperature, relative humidity, and cleanliness allow accurate and stable measurements [25]. The test-object used, an ad-hoc 3D artefact (

Figure 5), is characterized by important depth variations, different textures and materials, and the presence of both large scale and small scale details on the surfaces. The 3D scene includes contrast targets, scale bars and spheres. An interferometer-based scale bar is present in the laboratory and is used for the realization of the International System (SI) unit of length for laser trackers [26].

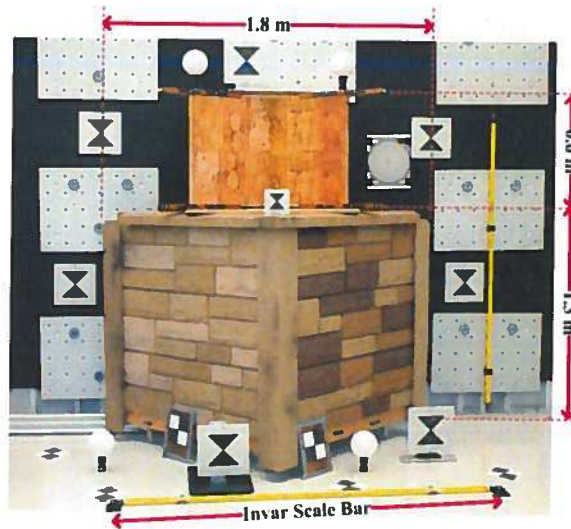


Figure 5. Test object in the environmentally controlled laboratory. The temperature in the laboratory is set at $20\text{ }^{\circ}\text{C} \pm 0.1\text{ }^{\circ}\text{C}$.

A Canon EOS 5D digital camera (4368×2912 pixels) equipped with a fixed focal length lens (Canon EF 50 mm f2.5 Compact Macro Lens) is used in the experiments. No automatic optical image stabilization is present. Two different angles of convergent images are tested (5° and 10°), again following a cross shape convergent configuration without the use of a stable mounting structure for giving a fixed baseline. The 3D artefact is acquired at a focusing distance of 4.75 m. The lens is glued so that its focus setting doesn't change. Aperture (f-stop) and ISO sensibility are kept fixed at f/8 and 100 respectively. A diffused and controlled ambient light (fluorescent) provides an illumination with reduced cast shadows.

3. Proposed Approach

3.1 Fundamental Questions in Metrology

There are three fundamental questions that we must answer when aspiring to work in metrology. These questions will appear obvious to a metrologist but in many fields outside metrology these are often overlooked or ignored. The first question is “how do you know what you are measuring?” This is the “measurand” issue in metrology. According to *VIM* [2], a measurand is the quantity intended to be measured. The measurand cannot be specified by a value but only by a description of a quantity. The set of quantity values being attributed to a given measurand, together with any other available relevant information, are the measurement results or results of measurement. Furthermore, a measurement result should be expressed as a single measured quantity value and a measurement uncertainty. This is not always the case in practice. Incidentally, according to *VIM* [2], accuracy is a qualitative term. Uncertainty should be used to express the accuracy of a measurement (the symbol u is typically used and in the case of an expanded uncertainty, U). For instance, in the field of computer vision, accuracy is frequently used as a quantitative term. Uncertainty is often linked to a deficiency with an algorithm.

The second question is “how do you know you can trust the measurement?” This is the calibration issue. According to *VIM* [2], a calibration is an “operation, under specified conditions, in a first step, establishes a relation between the quantity values with measurement uncertainties provided by measurement standards and corresponding indications with associated measurement uncertainties and, in a second step, uses this information to establish a relation for obtaining a measurement result from an indication.” For instance, a calibration function or a diagram is supplied under specified conditions. In photogrammetry, lens calibration which tries to mathematically model the image formation process in a real camera is usually supplied with a covariance matrix and other statistical information [31].

The third question is “how do you know measurements are equivalent?” This is the traceability issue and *VIM* [2] defines it as the property of a measurement result whereby the result can be related to a reference through a documented unbroken chain of calibrations, each contributing to the measurement uncertainty. Here both an uncertainty evaluation of a measurement result and an explicit connection to the meter in the case of dimensional metrology are required. For many technical and scientific communities working in dense 3D surface reconstruction, this is the main hurdle; cost being a major deterrent to its implementation. If we want to perform a correct evaluation of a particular 3D imaging system in a metrological context, all three questions must be answered. Furthermore, these three questions should be considered in metric surveys to develop an adequate understanding of the uncertainty components in measurement (as per *ISO 14253*).

3.2 Methodology of Data Comparison

Our accuracy tests are performed using ‘reference’ data acquired with two hemispherical laser scanners (LS1 and LS2), one total station (TS), one laser tracker (LT), and some contrast targets. Only the TS and LT have a clear measurement traceability route; the laser scanners may have one

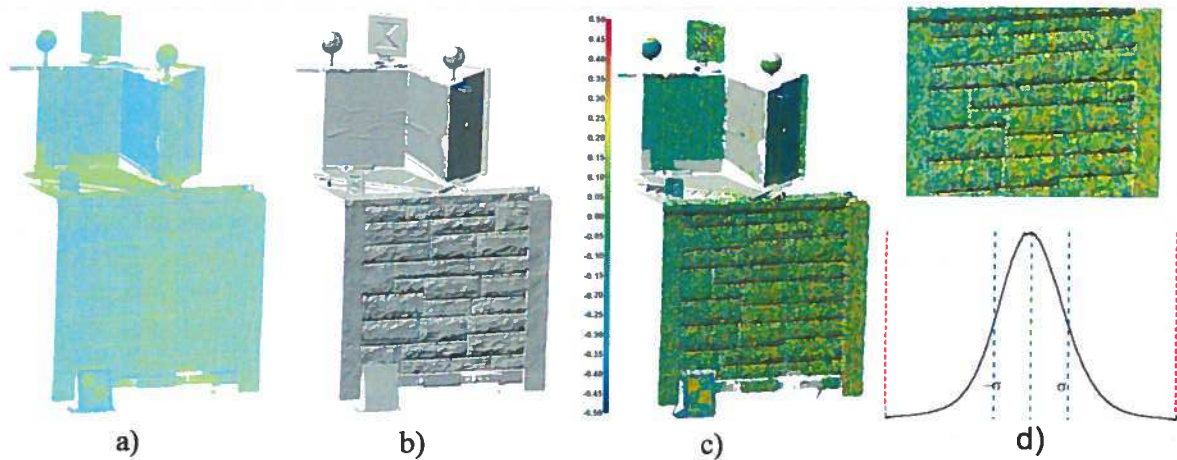
but no information is present in the manufacturer's data sheets. The two experiments are conducted according to the protocols presented in Section 2. Single 3D point clouds are measured in order to restrict the study to estimating the accuracy over a limited number of instrument stations. PolyWorks v12.1.18 IMAAlign™ software package from InnovMetric Software Inc.¹ provides the main image alignment and 3D point cloud comparison techniques. The alignment is based on an iterative algorithm that computes an optimal alignment by minimizing the 3D distances between common surface overlaps in a set of 3D images acquired from unknown viewpoints. One point cloud is fixed or set not to move during alignment. Here, a measurand can be defined based on that distance (signed value to denote direction). It is important to mention that the measurement uncertainty associated with that fixed point cloud is of the same order of magnitude as the other point clouds².

After each iteration, the algorithm applies to each 3D image a transformation matrix corrected by an incremental transformation matrix that best improves the image alignment with respect to the other 3D images. This incremental matrix is computed using a linear least-squares technique, and results from averaging the best alignment parameters of each image point in the overlapping surfaces. Incidentally, dual-axis inclination sensors are not operational in both laser scanners and hence could not be used in a constrained alignment. After convergence is reached, the alignment process is set to perform no iteration. Hence, we get a comparison between two 3D point clouds that have overlapping areas (

Figure 6a and 6b) and where the distance between those common overlapping surfaces is shown in

Figure 6c. A histogram and an error map of the image alignment errors bounded by a maximum acceptable distance error between 3D point clouds are generated (

Figure 6d).



¹ www.innovmetric.com (last accessed October 2014)

² On cooperative surfaces, the distribution of the distance differences follows closely a Gaussian distribution. The matter becomes more complex when surface curvature and sudden jumps in range values are present in a scene. In that case, the statistical distributions tend to be asymmetrical.

Figure 6. Images related to the alignment of two point clouds, a) the two aligned and colored point clouds, b) shaded representation, c) error map after comparison between two point clouds after alignment (color scale is ± 0.5 mm), d) histogram of the differences between point clouds and zoom on the error map after alignment (mean value = 0.0 mm and $\sigma = 0.25$ mm).

3.3 Instrumentation and Error Budget

A recently calibrated Leica FlexLine™ TS06plus Total Station is used to survey the contrast targets in the main entrance of the Cathedral in Marseille. The survey is performed from a single station in the morning when the wind is weak, the temperature is about $10\text{ }^{\circ}\text{C} \pm 2\text{ }^{\circ}\text{C}$, relative humidity is about $60\% \pm 10\%$ and the barometric pressure is fairly stable at $1019\text{ hPa} \pm 2\text{ hPa}$. The specification sheet quotes a distance measurement accuracy of $2\text{ mm} + 2\text{ ppm}$ (standard deviation as per *ISO-17123-4* and without reflector) and angle measurement (Hz, V) accuracy between $2''$ and $7''$ as per *ISO-17123-3*. The maximum distance between the TS and the scene is about 16.6 m. The uncertainty budget calculation shows that the main uncertainty contribution comes from the range distance estimation. The elevation and azimuth angular uncertainties at 16.6 m are about one quarter of the range uncertainty. The combined uncertainty at this distance is about $u_R(\text{TS}) = 2.18\text{ mm}$ (1σ) and expanded uncertainty $U_R(\text{TS}) = 4.49\text{ mm}$ ($k = 2$).

A Hemispherical FARO® Laser scanner³ Focus^{3D} model 120 (LS1) is used on that same entrance. Tests results from an experiment in laboratory conditions show that the standard deviation (1σ) of the residuals after fitting a plane equation to the data obtained on a cooperative planar surface with high reflectance and optimum scanner parameters gives a value of about 0.5 mm at a range of 6 m. This value represents the lowest measurement uncertainty value we may expect with this laser scanner. The manufacturer's specification sheet (*range noise*) quotes about half that value between 5 m and 10 m. This fact may be due to a different evaluation method and measurand. If we look at the alignment of two 3D point clouds acquired from two distinct distance positions in front of the main entrance and perform the comparison as described in the previous section, the 1σ value is about 1 mm. This number is selected as our local measurement uncertainty $u_R(\text{LS1}) = 1\text{ mm}$. This last value is a more realistic representation of the noise level present in the 3D point clouds for that type of surface. Already, we can see that the TS may become a limiting factor in the determination of the accuracy of any techniques in the present context. In a separate laboratory test, the LS1 lateral resolution is evaluated between 5 m and 20 m. With a contrast target characterized by a pattern with a spatial frequency of 5 lp/mm (lp: line pairs), the lateral resolution is between 1 mm and 2 mm at a range below 10 m. This is important in order to match the lateral resolution of laser scanner and dense 3D data.

In the laboratory at NRC Canada, an absolute distance meter (ADM)-based laser tracker model FARO® X is used to locate the contrast targets of the GCPs and Check Points (CPs) instead of a TS. Typically, specifications for laser trackers are given by an *ASME B89.4.19-2006* assessment where a maximum permissible error (MPE) is specified with a traceability route.

³ <http://www.faro.com/> (last visited October 2014)

Equation (1) gives the error when distance “L” is measured from the center of the instrument (0.1 m to 35 m),

$$E_{L,MPE} = \pm(20 \mu m + L \times 0.8 \mu m) . \quad (1)$$

This specification is an interval of measurement errors “...with respect to a known reference quantity value that is permitted by specifications or regulations for a given measurement, measuring instrument, or measuring system...” [2]. Metrologists interpret the MPE as a 3σ estimate. The MPE equation for this laser tracker is verified in the laboratory using an interferometer-based device *B89.7.5* where distances are measured using a displacement-measuring laser interferometer and spherically mounted retroreflector (SMR). The transverse capability of the laser tracker (elevation and azimuth angles) is given by

$$E_{T,MPE} = \pm(36 \mu m + L \times 6 \mu m) . \quad (2)$$

For a working distance of 4.75 m, the radial expanded ($k = 3$) uncertainty is approximately $U_R(LT) = 23.6 \mu m$ and the transverse expanded ($k = 3$) uncertainty is approximately $U_T(LT) = 64.5 \mu m$. The radial measuring capability of laser trackers in terms of uncertainty is much better than its angular measuring capability.

A hemispherical 3D scanner model Surphaser® 25HSX⁴ (LS2) is used in the laboratory. Tests results show that the 1σ noise after the alignment of two 3D point clouds acquired from two distinct distance positions in front of the ad-hoc 3D artefact gives a value of about 0.5 mm at a range of 5 m which is selected as our local measurement uncertainty, $u_R(LS2) = 0.5$ mm. This last value is again a more realistic representation of the noise level present in the 3D point clouds. Lateral resolution is evaluated using a star pattern and the lateral resolution is found to be near 0.5 mm at a range of 5 m.

A set of planar checkerboard targets and circular contrast targets (GCPs and CPs) are laser printed on self-adhesive sticker paper in A4 format. The geometric integrity of these paper targets is highly dependent on the humidity conditions present on-site (

Figure 7). We expect them to last for the day only. Other circular contrasts targets that are geometrically stable come with the laser scanner target kit. Other targets proprietary NRC contrast targets and spherical artefacts are used for checking the accuracy of the different instruments (

Figure 8). We expect the localization errors to originate from the acquisition process and the algorithms used to locate their center, and not from the physical integrity or material used (obviously within certain limits). Results are not reported here for brevity.

⁴ www.surphaser.com

3.4 Some Comments on the Error Budget Calculations

From the calculation shown above for a single point for the TS, an expanded uncertainty ($k = 2$) of 4.36 mm for radial measurements and 1.09 mm for angular measurements (at a distance of 16.6 m) are expected on the contrast targets. A local single 3D point expanded uncertainty for the LS1 of about 2 mm is anticipated on the entrance. In retrospect, a TS with a lower measurement uncertainty should have been used at the Marseille site.

The LT provides coordinates measurements with an uncertainty well below those achievable with both the Surphaser® laser scanner and the image-based technique being evaluated. From calculations, a combined expanded uncertainty ($k = 3$) of 0.069 mm for a 3D coordinates are expected on the proprietary NRC contrast targets. A local single 3D point expanded uncertainty for the LS2 of about 1 mm is anticipated on the surfaces of the 3D artefact. Incidentally, the coordinate values on the proprietary NRC targets are the only values where both uncertainty and traceability could be attached.

4. Results

4.1 Results Achieved in an Outdoor Environment

Both image correspondences and GCPs are employed in order to compute camera poses, orientations and scale. In particular, the registration of image-based results within the TS reference frame is achieved by using seven well-distributed planar targets. Internal orientation parameters, pre-computed within a calibration procedure performed with an ad-hoc image dataset not reported here, are refined in the process by adopting a Fraser-derived formulation [28]. Once orientations are defined, the 3D coordinates of nine CPs, visible in at least two images and back-projected into the 3D object space, are finally compared to the ones measured with the TS. This accuracy assessment is performed starting from all available acquisition protocols. Final standard deviations, σ ($k = 1$), are listed in Table 1. Results achieved by the 60 mm lens are generally better than the corresponding ones gathered by the 24 mm lens. This is due in part to the better range and lateral accuracy provided by longer focal length, according to triangulation equations [24]. Also, the combined data sets (highlighted in yellow) show the best metric performance. Incidentally, $k = 1$ is used in order to allow a comparison with current literature in photogrammetry.


24 mm lens				
A	Number of Images	σ_x (mm)	σ_y (mm)	σ_z (mm)
3°	5	11.9	15.4	12.6
5°	3	20.6	28.6	14.3
10°	3	18.9	27.7	24.2
3° + 5° + 10°	9	9.0	13.2	11.3
60 mm lens				
A	Number of	σ_x (mm)	σ_y (mm)	σ_z (mm)

	Images			
3°	5	9.2	13.5	5.8
5°	3	18.7	16.5	20.8
10°	3	14.5	15.9	14.3
3°+5°+10°	9	4.8	2.2	4.6
24 + 60 mm lenses				
A	Number of Images	σ_x (mm)	σ_y (mm)	σ_z (mm)
3° + 5° + 10°	29	2.9	2.1	3.1

Table 1. Accuracy assessment of the image orientation phase: nine CPs measured with a total station (TS) characterized by $u_R(TS) = 2.18$ mm (Cathédrale de la Major).

Depth maps are then extracted, after having selected the best parametrical setup in accordance with the scene characteristics (see

Figure 2). In particular, many tests are carried out in order to deepen our understanding of three chief parameters, i.e. the regularization factor, the Z-quantification factor and the final Z-resolution [29]. A metric evaluation of the dense image matching accuracy is finally performed through two different studies. Point clouds are first analyzed with the software PolyWorks: best-fit geometrical primitives are thereby extracted from significant portions of the acquired 3D scene, such as planar surfaces (e.g. pillar) and cylinders (e.g. columns). Resulting standard deviations values are then evaluated. Secondly, the metrological assessment is completed by performing comparisons with the ‘reference’ data set, i.e. the point cloud acquired with the FARO® Laser scanner Focus^{3D} (LS1) at a mean instrument-object distance equal to 5 m. The tests are carried out within the software PolyWorks, after having registered the LS1 data with the image-based point cloud. Three significant portions of the symmetrical test-object are selected for the comparisons. For each subset, standard deviations, σ ($k = 1$), of the distances between the compared point clouds and the corresponding histograms are computed. Results are listed in Table 2. The best accuracy level (highlighted in yellow) is delivered by the data set including images acquired by both lenses. In this case, a standard deviation below half a centimeter is achieved.

24 mm lens			
α	Number of Images	σ (mm)	Histogram
3°	5	7.65	
5°	3	6.66	
10°	3	6.22	
3° + 5° + 10°	9	4.83	
60 mm lens			
α	Number of Images	σ (mm)	Histogram






3°	5	8.38	
5°	3	8.34	
10°	3	7.14	
3° + 5° + 10°	9	5.07	
24 + 60 mm lenses			
α	Number of Images	σ (mm)	Histogram
3° + 5° + 10°	29	3.73	

Table 2. Statistics delivered by comparisons performed on the 3D point cloud on one half of the portal. LS1 was used to acquire the point cloud and is characterized by $u_R(\text{LS1}) = 1$ mm (Cathédrale de la Major).

The color-coded map associated with this acquisition protocol is shown in

Figure 7, together with a view of the compared 3D scene. The color scale ranges from -10 mm (blue) to 10 mm (red). The error distribution shows that the areas delivering the largest deviations are mainly areas subject to cast shadows, area characterized by dark and homogeneous textures, such as the dark pattern of the pillar, and, marble columns, where the computed differences are negative. This last problem is connected to the performance of time-of-flight laser scanners in the presence of translucent surfaces. Here, an apparent depth penetration of 5 to 6 mm is observed [30]. Current commercial laser scanners don't compensate for these types of systematic errors, at least in the versions delivered to typical customers.

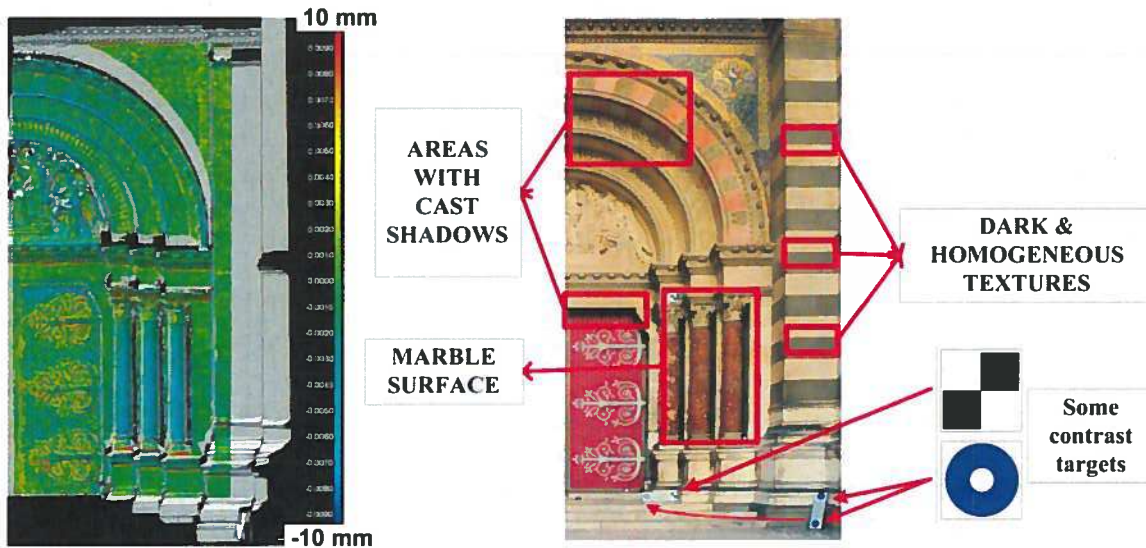


Figure 7. 3D point cloud on one half of the portal. Left: color-coded map delivered by comparison, right: the resulting problematic areas specified on the color image.

4.2 Results in an Environmentally Controlled Laboratory

Once image correspondences and relative orientations are computed, the datum ambiguity is solved by using four well-distributed GCPs. The latter are selected within the proprietary NRCTargets measured with the LT: the same data are employed to register also the LS2-acquired point clouds in the same LT reference frame. Camera calibration parameters are computed by performing a self-calibration within the bundle adjustment procedure. This step occurs just before the dense multi-image matching phase (

Figure 1). In order to evaluate the metric accuracy of the photogrammetric orientation results, the remaining 10 targets (contrast and proprietary NRC targets) are then assumed as independent check points and matched in at least three images. Their 3D coordinates, thereby computed as intersections of homologous rays, are finally compared to the ones measured with the LT and LS2, delivering the standard deviations, σ ($k = 1$), listed in Table 3.

50 mm lens				
α	Number of Images	σ_x (mm)	σ_y (mm)	σ_z (mm)
5°	15	0.42	0.60	0.36
10°	15	0.49	0.80	0.32
5° + 10°	27	0.47	1.34	0.40

Table 3. Accuracy assessment of image orientation phase, $u_R(LT) = 0.047$ mm and $u_R(LS2) = 0.5$ mm.

Results show that the orientation algorithm achieves a considerably good accuracy level: all standard deviations are below 1 mm, with the exception of one value. Furthermore, results are consistent with the measurement uncertainty of both LT and LS2. Hypothesis testing, not used here, can help for a documented decision process. By analyzing the individual residuals, the higher deviations correspond to a few targets lying on the floor, whose position requires an unfavorable acquisition direction for all the instruments employed.

Depth maps are then extracted, by adopting the best parametrical setup, selected in accordance with the scene characteristics. This step is performed within the dense multi-image matching phase (

Figure 1). Starting from orientations, depth values, origin and steps of depth quantification, point clouds are finally delivered in PLY file format [29].

Figure 8 shows the result achieved with the 5°-dataset. The raw image-based point clouds are then compared with measured ‘reference’ data, i.e. the 3D point cloud acquired with the LS2. The tests are performed within the software PolyWorks. No alignment is necessary, just a straight comparison is performed in the software (iteration set to 0). The standard deviations, σ ($k = 1$), of the distances between the compared entities and corresponding histograms are listed in Table 4.

50 mm lens




α	Number of Images	σ (mm)	Histogram
5°	15	0.88	
10°	15	0.67	
5° + 10°	27	0.67	

Table 4. Statistics delivered by comparisons, $u_R(\text{LS2}) = 0.5$ mm.

The dense image matching algorithm is able to reach the same accuracy level previously pointed out by the orientation metrological assessment: all tests, in fact, deliver sub-millimeter standard deviations and comparable results. The distance difference histograms are fairly symmetrical and closely follow a Gaussian distribution. The method is explained in Section 3.2.

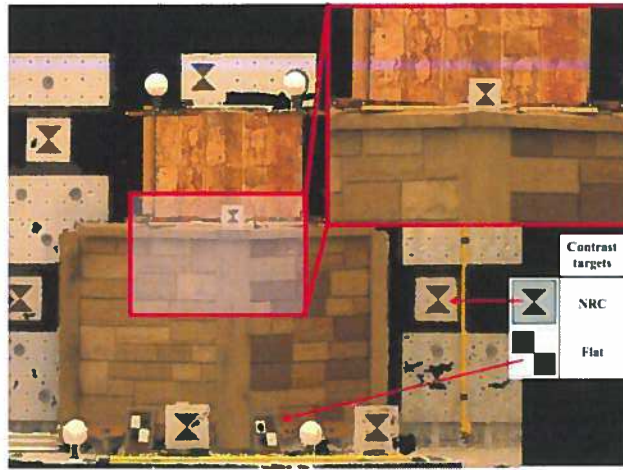


Figure 8. The colored point cloud extracted with the 5° data set on the ad-hoc 3D artefact.

Furthermore, the color-coded error maps show that the largest deviations from the reference data are mainly located at sharp surface gradients, such as the ones corresponding to the edges between the vertical walls of the corners and to the small grooves among the bricks. As explained earlier, these are similar to sudden changes of curvature and depth on the surface object. As evidence, the distance difference (error) distribution associated to results achieved with the 5° data set is shown in

Figure 9: the color scale ranges from -5 mm (violet) to +5 mm (red). These sharp edges are problematic for active laser scanners as well. This is especially true when the spot diameter is large compared to the structural (lateral) resolution being analyzed. In the present situation, there may be a mismatch between the structural resolution of the LS and the image-based 3D point clouds.

Figure 9 shows that the image-based reconstruction can resolve small creases on the glued surfaces (top section).

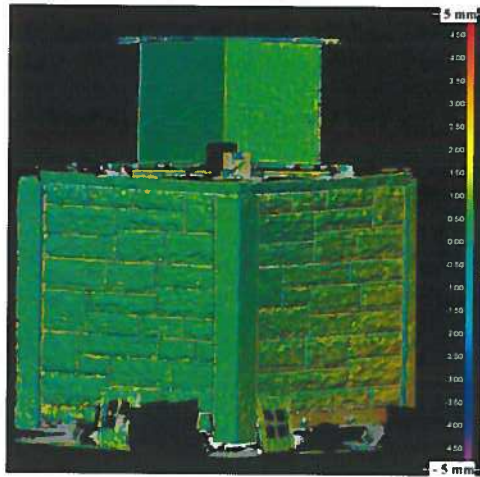


Figure 9. Color-coded map delivered by comparison.

5. Conclusions

An increasingly number of software solutions for the automatic generation of textured dense 3D point clouds from a set of unoriented images has recently appeared in the market. So far this development has not been supported by the definition of clear standards and guidelines that are necessary to evaluate the resolution, repeatability, reproducibility and measurement uncertainty of a given solution. It is within this context that this paper strives to provide an approach to assess both the metric quality and limitations of a particular image-based 3D modelling technique and that within a metrological context. The metrological approach adopted here is based on the use of reference instruments, whose uncertainty is estimated through both specifications and experimental tests. Of particular concern, we point out that the metric quality of 3D ‘reference’ data originating from active 3D imaging systems need to be questioned and hence verified beforehand. The approach presented is applied to the metric evaluation of the algorithmic solutions implemented in the IGN’s suite of tools (Apero/MicMac); in particular, the influence of the image acquisition protocol used is studied in some depth, by examining its effects on the orientation and dense matching phases. Two experiments are carried out, in order to analyze the software performance in dealing with both outdoor and environmentally controlled conditions for the case of a single 3D image. The results achieved within these two contexts are not general since they are of course influenced by the specific operating conditions affecting each case study, i.e. data sets, hardware/software means, ambient and operators. Nevertheless, these studies offer a promising procedural workflow that can be further applied to different case studies in order to set specifically-adoptable best practices. Aspects of metrological nature should be developed further for the good of the different communities and for market growth. These aspects include defining what the measurand is in a given comparison, how calibration is performed and how often, what the traceability route is that links a measurement value to the SI unit, and, finally how the measurement accuracy of a system is quoted. Many of these issues, some well documented and others still open, offer great opportunities for research and development for academia, national metrology institutes, and industry.

6. Acknowledgements

The authors would like to acknowledge the staff members of the UMR 3495, MAP-CNRS whose hard efforts made the work on-site possible. Many thanks go to Marc-Pierrot Deseilligny for the suggestions regarding the use of the IGN software suite. We would like to thank the CNRS and French Embassy in Ottawa in Canada for providing financial support. Further support was provided by the Culture 3D Clouds project within the framework of the French national plan "Investment for the future - technology development for digitizing cultural, scientific and educational content".

7. References

- [1] F. Remondino, S. Del Pizzo, T. Kersten, and S. Troisi, "Low-cost and open-source solutions for automated image orientation – A critical overview," *Progress in Cultural Heritage Preservation: Lecture Notes in Computer Science*, vol. 7616, pp. 40–54, 2012.
- [2] JCGM, "International vocabulary of metrology," 3rd edition, *JCGM 200*, 2012.
- [3] JCGM, "Evaluation of measurement data – Guide to the expression of uncertainty in measurement," *JCGM 100*, 2008.
- [4] ASTM (E57), "Committee E57 on 3D Imaging Systems," *ASTM International*.
- [5] ISO, "Geometrical Product Specifications (GPS) - Acceptance and reverification tests for coordinate measuring machines (CMM)," *ISO 10360*, 2011.
- [6] ISO, "Optics and optical instruments – Field procedures for testing geodetic and surveying instruments," *ISO 17123*, 2014.
- [7] VDI, "Optical 3D measuring systems - Optical systems based on area scanning," Part 2, *VDI/VDE 2634*, 2012.
- [8] ISO, "Geometrical product specifications (GPS) - Inspection by measurement of workpieces and measuring equipment -- Part 1: Decision rules for proving conformity or nonconformity with specifications -- Part 2: Guidance for the estimation of uncertainty in GPS measurement, in calibration of measuring equipment and in product verification," *ISO 14253*, 2013.
- [9] S. El-Hakim, J.-A. Beraldin, and F. Blais, "Critical Factors and Configurations for Practical 3D Image-Based Modeling," *Proceedings of 6th Conf. on 3D Measurement Techniques*, Zurich, Switzerland, pp. 159–167, 2003.

- [10] K. Wenzel, M. Rothermel, D. Fritsch, and N. Haala, "Image acquisition and model selection for multi-view stereo," *Proceedings of 3D-ARCH – 3D Virtual Reconstruction and Visualization of Complex Architectures*, Trento, Italy, pp. 251-258, February 2013.
- [11] P. Waldhäusl and C. Ogleby, "3 x 3 Rules for simple photogrammetric documentation of architecture," *International Archives of Photogrammetry and Remote Sensing*, Melbourne, Australia, vol. 30, no. 5, pp. 426-429, 1994.
- [12] EuroSDR, <http://www.eurosd.net>, (last accessed 10/27/2014).
- [13] D. Scharstein and R. Szeliski, "A Taxonomy and Evaluation of Dense Two-Frame Stereo Correspondence Algorithms," *Int. J. Comput. Vision*, vol. 47, no. 1-3, pp. 7-42, 2002.
- [14] S. Seitz, B. Curless, J. Diebel, D. Scharstein, and R. Szeliski, "A comparison and evaluation of multi-view stereo reconstruction algorithms," *Proceedings of IEEE Computer Society Conference on Computer Vision and Pattern Recognition*, New York, NY, vol. 1, pp. 519-528, June 2006.
- [15] A. Ahmadabadian, S. Robson, J. Boehm, M. Shortis, K. Wenzel and D. Fritsch, "A comparison of dense matching algorithms for scaled surface reconstruction using stereo camera rigs," *ISPRS J. Photogramm*, vol. 78, no. 4, pp. 157-167, 2013.
- [16] A. Georgantas, M. Brédif, and M. Pierrot-Deseilligny, "An accuracy assessment of automated photogrammetric techniques for 3D modelling of complex interiors," *Proceedings of XXII ISPRS Congress*, Melbourne, Australia, pp. 23-28, August-September 2012.
- [17] N. Pears, Y. Liu, and P. Bunting, *3D Imaging, Analysis and Applications*, Springer-Verlag, London, UK, 2012.
- [18] G. Vosselman and H. Mass, *Airborne and Terrestrial Laser Scanning*, Whittles Publishing, Scotland, UK, 2010.
- [19] M. Pierrot-Deseilligny and I. Clery, "APERIO, an open-source bundle adjustment software for automatic calibration and orientation of set of images," *Proceedings of 3D-ARCH – 3D Virtual Reconstruction and Visualization of Complex Architectures*, Trento, Italy, pp. 269-277, March 2011.
- [20] M. Pierrot-Deseilligny and N. Paparoditis, "A multiresolution and optimization-based image matching approach: an application to surface reconstruction from SPOT5-HRS stereo imagery," *Proceedings of the ISPRS Workshop on Topographic Mapping from Space*, Ankara, Turkey, pp. 73-77, 2006.

- [21] A. Vedaldi and B. Fulkerson, "VLFeat: An Open and Portable Library of Computer Vision Algorithms," *Proceedings of the International Conference on Multimedia*, Firenze, Italy, pp. 1469-1472, 2010.
- [22] B. Triggs, P. McLauchlan, R. Hartley, and A. Fitzgibbon, "Bundle Adjustment – A Modern Synthesis," in *Vision Algorithms: Theory and Practice*, A. Zisserman, and R. Szeliski, (eds.), Springer-Verlag, Berlin Heidelberg, Germany, 2000.
- [23] M. Drouin, M. Trudeau, and S. Roy, "Geo-consistency for wide multi-camera stereo - Computer Vision and Pattern Recognition," *Proceedings of IEEE Computer Society Conference on Computer Vision and Pattern Recognition*, San Diego, California, vol.1, pp. 351–358, June 2005.
- [24] F. Blais and J.-A. Beraldin, "Recent Developments in 3D Multi-modal Laser Imaging Applied to Cultural Heritage," *Mach. Vision Appl.*, vol. 17, no. 6, , pp. 395–409, 2006.
- [25] J.-A. Beraldin, M. Rioux, L. Cournoyer, F. Blais, M. Picard, and J. Pekelsky, "Traceable 3D imaging metrology," *P. SPIE IS & T Elect. Im.*, vol. 6491, Videometrics IX, 11 p., January 2007.
- [26] ASME, "Metrological Traceability of Dimensional Measurements to the SI Unit of Length," *ASME B89.7.5*, 2006.
- [27] ASME, "Performance Evaluation of Laser-Based Spherical Coordinate Measurement Systems," *ASME B89.4.19*, 2006.
- [28] C. Fraser, "Photogrammetric Camera Component Calibration: A Review of Analytical Techniques," in *Calibration and Orientation of Cameras in Computer Vision*, A. Grün and T.S. Huang (eds.), Springer Series in Information Sciences, Berlin, Germany, 2001.
- [29] MicMac Documentation, <http://logiciels.ign.fr> (last accessed 10/9/2014).
- [30] S. El-Hakim, J.-A. Beraldin, M. Picard, and L. Cournoyer, "Surface reconstruction of large complex structures from mixed range data - The Erechtheion experience," *Proceedings of XXXVII ISPRS Congress*, Beijing, China, part. B5, pp. 1077–1082, July 2008.
- [31] M. Cooper and S. Robson, "Theory of Close Range Photogrammetry," chap. 2 in *Close Range Photogrammetry and Machine Vision*, K. Atkinson (ed.), Whittles Publishing, Scotland, UK, pp. 9-51, 2001.